Nonlinear optical generation with reduced absorption using electric-field coupling in atomic hydrogen

K. Hakuta,* L. Marmet, and B. P. Stoicheff
Department of Physics, University of Toronto, Toronto, Ontario, Canada M5S 1A7
and Ontario Laser and Lightwave Research Centre, Toronto, Ontario, Canada M5S 1A7
(Received 28 August 1991)

Resonantly enhanced second-harmonic generation in atomic hydrogen was investigated near 121.6 nm. With the application of a dc electric field, it is shown that coupling of the 2*s* and 2*p* states produces resonantly enhanced nonlinear susceptibility and reduced absorption at the second-harmonic wavelength, resulting in an increased net efficiency of the second-harmonic-generation process.

PACS number(s): 42.65.Ky, 42.50.−p, 32.60.+i

I. INTRODUCTION

Considerable discussion has recently taken place concerning the possibility of obtaining stimulated emission without population inversion [1–9]. In 1989, Harris developed a theory [2] to show that when two upper levels of a four-level system are purely lifetime broadened and decay to the same continuum, there will be a destructive interference in the absorption profile of lower-level atoms which is not present in the stimulated emission profile of upper level atoms, thus resulting in laser gain without inversion. It was noted that this theory holds for lifetime broadening of the two upper levels caused by autoionization, tunneling, or radiative decay. In the above processes, the upper levels are coupled by spontaneous decay to the same final continuum or discrete level. However, it was also predicted [6] that transparency could be induced by active coupling of the two upper levels with a strong electromagnetic field. More recently, Harris, Field, and Imamoğlu [8] extended these concepts to nonlinear processes and showed that the application of a strong electromagnetic field between metastable and upper states can resonantly enhance the nonlinear susceptibility of the medium and at the same time induce transparency and a zero in the contribution of the resonance transition to the refractive index. Moreover, they predicted that many orders of improvement in conversion efficiency could be achieved because of the induced transparency.

In a recent paper [10], we demonstrated that coupling of the metastable and upper levels by an applied dc electric field yields the same characteristics predicted by Harris, Field, and Imamoğlu [8] for coupling with an electromagnetic field. In addition, experimental evidence was given using the behavior of second-harmonic generation (SHG) that coupling of the 2*s* and 2*p* states in atomic hydrogen leads to reduction in absorption at the center of the Stark-split components. In the present paper, we give a detailed outline of the theory applicable to SHG with reduced absorption using electric-field coupling of the 2*s* and 2*p* states of atomic hydrogen. The experimental procedures are described, and the observed results are compared with theoretical predictions.

II. THEORY

A. Derivation of the density-matrix equations

In an external field, SHG in atomic systems is possible via the third-order nonlinear susceptibility. Such an electric-field-induced SHG may also be treated as a second-order process where the electric field is explicitly included in the expression for $\chi^{(2)}$. Here, we have chosen the latter method, and calculate the polarization using the density-matrix formalism with a decoupled basis set of three discrete levels $|1\rangle$, $|2\rangle$, and $|3\rangle$ having energies $\hbar\omega_1$, $\hbar\omega_2$, and $\hbar\omega_3$, respectively.

An energy-level diagram of the system is shown in Fig. 1. A strong electric field E_{dc} is applied to the atom to couple the metastable state $|2\rangle$ with state $|3\rangle$ which radiatively decays to $|1\rangle$ with a rate Γ. A laser field of frequency ω_a is incident on the atom, and radiation at

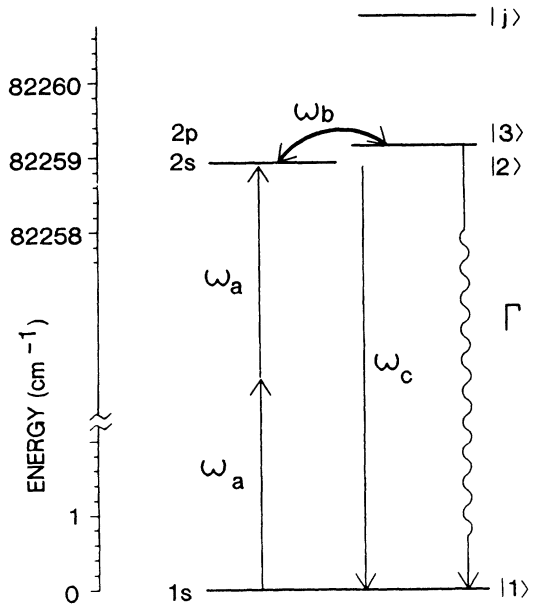

FIG. 1. Energy-level diagram for electric-field induced second-harmonic generation at $\omega_c = 2\omega_a + \omega_b$. The vertical scale on the left shows the energies relevant to atomic hydrogen.

$\omega_c = 2\omega_a$ is produced by SHG. Values of the linear and nonlinear susceptibilities $\chi^{(1)}$ and $\chi^{(2)}$ are derived from the polarization induced by the electromagnetic fields of frequencies ω_a and ω_c and the dc electric field (of frequency $\omega_b = 0$). The Hamiltonian for the system is defined as $H = H_0 + H_i$, where H_0 is the field-free Hamiltonian and H_i is the interaction of the atom with the electric and electromagnetic fields. These individual contributions may be expressed as the following matrix elements:

$$H_i^{32} = -\mu_{32} E_{\rm dc} = -\hbar\Omega_{32} , \tag{1a}$$

$$H_i^{31} = -\tfrac{1}{2}\mu_{31} E_{\omega_c} e^{-i\omega_c t} = -\tfrac{1}{2}\hbar\Omega_{31} e^{-i\omega_c t} , \tag{1b}$$

$$H_i^{21} = -\sum_j \frac{\mu_{2j}\mu_{j1}}{4\hbar} \frac{E_{\omega_a}^2 e^{-i\omega_c t}}{\omega_j - \omega_a} = -\tfrac{1}{2}\hbar\Omega_{21} e^{-i\omega_c t} . \tag{1c}$$

Here, the rotating-wave approximation was used, and only resonant terms have been included; the $\mu_{mn} = e\langle m|z|n\rangle$ are dipole-moment matrix elements for the transition $m \leftrightarrow n$ with linear polarization, Ω_{ij} are the Rabi frequencies, and E_ω are the amplitudes of the electromagnetic fields. In Eq. (1a), Ω_{32} is the dc Stark shift; in Eq. (1c), the summation is taken over all intermediate states $|j\rangle$. We define Ω_{21} as an effective Rabi frequency obtained from perturbation theory, and $\mu_{12} = \hbar\Omega_{12}/E_{\omega_a}$ as the corresponding effective dipole moment.

The time-varying density-matrix elements are given by

$$\frac{d\rho_{11}}{dt} = -\frac{i}{\hbar}(H_i^{12}\rho_{21} - H_i^{21}\rho_{12} + H_i^{13}\rho_{31} - H_i^{31}\rho_{13}) + \Gamma\rho_{33} , \tag{2a}$$

$$\frac{d\rho_{22}}{dt} = -\frac{i}{\hbar}(H_i^{21}\rho_{12} - H_i^{12}\rho_{21} + H_i^{23}\rho_{32} - H_i^{32}\rho_{23}) , \tag{2b}$$

$$\frac{d\rho_{33}}{dt} = -\frac{i}{\hbar}(H_i^{31}\rho_{13} - H_i^{13}\rho_{31} + H_i^{32}\rho_{23} - H_i^{23}\rho_{32}) - \Gamma\rho_{33} , \tag{2c}$$

$$\frac{d\rho_{21}}{dt} = -i(\omega_2 - \omega_1)\rho_{21} - \frac{i}{\hbar}(H_i^{21}\rho_{11} + H_i^{23}\rho_{31} - H_i^{21}\rho_{22} - H_i^{31}\rho_{23}) , \tag{2d}$$

$$\frac{d\rho_{31}}{dt} = -i(\omega_3 - \omega_1)\rho_{31} - \frac{i}{\hbar}(H_i^{31}\rho_{11} + H_i^{32}\rho_{21} - H_i^{21}\rho_{32} - H_i^{31}\rho_{33}) , \tag{2e}$$

$$\frac{d\rho_{32}}{dt} = -i(\omega_3 - \omega_2)\rho_{32} - \frac{i}{\hbar}(H_i^{31}\rho_{12} + H_i^{32}\rho_{22} - H_i^{12}\rho_{31} - H_i^{32}\rho_{33}) . \tag{2f}$$

We then define the matrix σ by $\rho_{11} = \sigma_{11}$, $\rho_{22} = \sigma_{22}$, $\rho_{33} = \sigma_{33}$, $\rho_{21} = \sigma_{21} e^{-i2\omega_a t}$, $\rho_{31} = \sigma_{31} e^{-i\omega_c t}$, and $\rho_{32} = \sigma_{32}$. On substitution in Eqs. (2), we obtain for the off-diagonal elements

$$\frac{d\sigma_{21}}{dt} = -i\Delta\omega_{21}\sigma_{21} + i[\tfrac{1}{2}\Omega_{21}(\rho_{11} - \rho_{22}) - \tfrac{1}{2}\Omega_{31}\sigma_{23} + \Omega_{23}\sigma_{31}] , \tag{3a}$$

$$\frac{d\sigma_{31}}{dt} = -i\Delta\omega_3\sigma_{31} + i[\tfrac{1}{2}\Omega_{31}(\rho_{11} - \rho_{33}) - \tfrac{1}{2}\Omega_{21}\sigma_{32} + \Omega_{32}\sigma_{21}] , \tag{3b}$$

$$\frac{d\sigma_{32}}{dt} = -i\Delta\omega_{32}\sigma_{32} + i[\Omega_{32}(\rho_{22} - \rho_{33}) + \tfrac{1}{2}\Omega_{31}\sigma_{12} - \tfrac{1}{2}\Omega_{12}\sigma_{31}] . \tag{3c}$$

Here, the frequency detunings are $\Delta\omega_{21} = \omega_2 - \omega_1 - 2\omega_a$, $\Delta\omega_{31} = \omega_3 - \omega_1 - \omega_c$, and $\Delta\omega_{32} = \omega_3 - \omega_2 - \omega_b$. By introducing phenomenological decay rates in the off-diagonal terms, the detunings can be expressed as complex values $\Delta\tilde{\omega}_{21} = \Delta\omega_{21}$, $\Delta\tilde{\omega}_{31} = \Delta\omega_{31} - (i/2)\Gamma$, and $\Delta\tilde{\omega}_{32} = \Delta\omega_{32} - (i/2)\Gamma$. Steady-state solutions are obtained by setting the time derivatives given in Eqs. (3) equal to zero. These yield

$$\sigma_{21} = \frac{\Delta\tilde{\omega}_{31}\Omega_{21}(\rho_{11} - \rho_{22}) + \Omega_{23}\Omega_{31}(\rho_{11} - \rho_{33}) - \xi_2\Omega_{23}(\rho_{22} - \rho_{33})}{2\Delta\tilde{\omega}_{21}\Delta\tilde{\omega}_{31} - 2|\Omega_{32}|^2} , \tag{4a}$$

$$\sigma_{31} = \frac{\Delta\tilde{\omega}_{21}\Omega_{31}(\rho_{11} - \rho_{33}) + \Omega_{32}\Omega_{21}(\rho_{11} - \rho_{22}) - \xi_3\Omega_{32}(\rho_{22} - \rho_{33})}{2\Delta\tilde{\omega}_{21}\Delta\tilde{\omega}_{31} - 2|\Omega_{32}|^2} , \tag{4b}$$

$$\sigma_{32} = \frac{1}{2\Delta\tilde{\omega}_{32}}[2\Omega_{32}(\rho_{22} - \rho_{33}) + \Omega_{31}\sigma_{12} - \Omega_{12}\sigma_{31}] , \tag{4c}$$

where $\xi_2 = \Delta\tilde{\omega}_{31}\Omega_{31}/\Delta\tilde{\omega}_{32}^* + \Omega_{21}\Omega_{32}/\Delta\tilde{\omega}_{32}$ and $\xi_3 = \Delta\tilde{\omega}_{21}\Omega_{21}/\Delta\tilde{\omega}_{32} + \Omega_{31}\Omega_{23}/\Delta\tilde{\omega}_{32}^*$. Here we have assumed a strong dc field so that $|\Omega_{32}| \gg |\Delta\tilde{\omega}_{32}|$, and weak electromagnetic fields so that $|\Omega_{31}|$ and $|\Omega_{21}|$ are much smaller than the detunings $|\Delta\tilde{\omega}_{32}|$ and $|\Delta\tilde{\omega}_{31}|$. It may be noted that under conditions of weak electromagnetic fields, the steady-state populations are $\rho_{11} \simeq 1$ and $\rho_{22}, \rho_{33} \simeq 0$. In this case, terms containing the factor $(\rho_{22} - \rho_{33})$ in Eqs. (4a) and (4b) can be neglected.

B. Calculation of the susceptibilities $\chi^{(1)}$ and $\chi^{(2)}$

The single atom polarization is given by

$$\langle\mu\rangle = \mathrm{Tr}[\rho\mu] = \mu_{13}\sigma_{31} e^{-i\omega_c t} + \mu_{12}\sigma_{21} e^{-i2\omega_a t} + \mu_{23}\sigma_{32} + \text{c.c.} , \tag{5}$$

where the terms on the right-hand side arise from one-photon emission and absorption, two-photon emission and absorption, and the dipole moment induced by E_{dc}, and c.c. denotes their respective complex conjugates. The macroscopic polarization at ω_c is given in terms of the susceptibilities by

$$P(\omega_c)=N\langle\mu(\omega_c)\rangle=\epsilon_0\chi^{(1)}(-\omega_c;\omega_c)E_{\omega_c} + \tfrac{1}{2}\epsilon_0\chi^{(2)}(-\omega_c;\omega_a,\omega_a)E_{\omega_a}E_{\omega_a} , \tag{6}$$

where N is the atom density. We equate the terms proportional to E_{ω_c} and $E_{\omega_a}E_{\omega_a}$ of Eq. (5) with the corresponding terms of Eq. (6), and using Eq. (4b) obtain the expressions for $\chi^{(1)}$ and $\chi^{(2)}$, respectively,

$$\chi^{(1)}(-\omega_c;\omega_c)=\frac{N}{2\epsilon_0\hbar}\frac{\Delta\tilde{\omega}_{21}}{\Delta\tilde{\omega}_{21}\Delta\tilde{\omega}_{31}-|\Omega_{32}|^2}\mu_{13}\mu_{31} , \tag{7}$$

$$\chi^{(2)}(-\omega_c;\omega_a,\omega_a)=\frac{N}{\epsilon_0\hbar^2}\frac{\Omega_{32}}{\Delta\tilde{\omega}_{21}\Delta\tilde{\omega}_{31}-|\Omega_{32}|^2} \times\mu_{13}\sum_j\frac{\mu_{2j}\mu_{j1}}{\omega_j-\omega_a} . \tag{8}$$

It is clearly seen from Eqs. (7) and (8) that completely different behaviors are expected for linear and nonlinear susceptibilities. For instance, $\chi^{(1)}(-\omega_c;\omega_c)$ takes a zero value at the two-photon resonant frequency $\omega_c=\omega_2-\omega_1\equiv\omega_{21}$. That is, perfect transparency can be induced by the dc electric field since $\Delta\tilde{\omega}_{21}=0$. On the other hand, $\chi^{(2)}(-\omega_c;\omega_a,\omega_a)$ may have a reasonably large value at $\omega_c=\omega_{21}$. As shown below, these results provide the possibility for enormous increase in generating SH radiation.

C. Significance of induced transparency

In SHG, the electric field of the generated wave is driven by the nonlinear polarization and is described by the propagation equation:

$$\frac{\partial^2E_{\omega_c}}{\partial z^2}+\frac{\omega_c^2}{c^2}[1+\chi^{(1)}(-\omega_c;\omega_c)]E_{\omega_c}=-\mu_0\omega_c^2P(\omega_c) . \tag{9}$$

This equation is solved by neglecting the depletion of the incident wave and by using the boundary condition $E_{\omega_c}=0$ at $z=0$ to give

$$E_{\omega_c}=-\frac{1}{2}\frac{\chi^{(2)}(-\omega_c;\omega_a,\omega_a)}{\chi^{(1)}(-\omega_c;\omega_c)} \times\left[1-\exp\left[i\frac{\omega_c}{2c}\chi^{(1)}(-\omega_c;\omega_c)z\right]\right] \times E_{\omega_a}^2\exp(ik_{\omega_c}z) . \tag{10}$$

Here, we assume that the medium is transparent to the incident wave, i.e., $\chi^{(1)}(-\omega_a;\omega_a)=0$. This expression describes the generated wave as a superposition of a driven wave and a freely propagating wave in the medium. If the medium has nonzero absorption for the generated wave, the free wave is damped out after a long propagation path, while the amplitude of the generated wave first increases and then reaches a stationary value E_S as it propagates through the medium. An ultimate conversion efficiency η of the SHG process can be defined as

$$\eta=\left|\frac{E_S}{E_{\omega_a}}\right|^2=\frac{1}{4}\left|\frac{\chi^{(2)}(-\omega_c;\omega_a,\omega_a)}{\chi^{(1)}(-\omega_c;\omega_c)}E_{\omega_a}\right|^2 \propto\left|\frac{\Omega_{32}}{\Delta\tilde{\omega}_{21}}\right|^2 . \tag{11}$$

This clearly shows that with $\Delta\tilde{\omega}_{21}\to0$, an extremely high conversion efficiency can be achieved at the two-photon resonant frequency. Also, it should be mentioned that the phase-matching condition $\mathrm{Re}[\chi^{(1)}(-\omega_a;\omega_a)]=0$ is exactly satisfied at the two-photon resonant frequency since the real part of $\chi^{(1)}$ gives a zero in the contribution of the resonance transition to the refractive index.

In practice, the inhomogeneous or Doppler broadening must be included in the calculation by convolving the susceptibilities $\chi^{(1)}$ and $\chi^{(2)}$ over the Gaussian density of states. The transparency is no longer perfect under these conditions. However, the linear susceptibility at $\omega_c=\omega_{21}$ can be reduced to nearly zero by increasing the electric field to a value such that Ω_{32} exceeds the width of the wings of the Doppler profile. In the above theory, collisional effects have been neglected.

The requirement of a strong dc field for the derivation of Eqs. (4) results in the condition $E_{dc}\gg1$ kV/cm. This causes no problem since $E_{dc}>10$ kV/cm is needed to separate the Stark components by a splitting larger than the Doppler breadth (~1.4 cm^{-1}). The second condition requires weak electromagnetic fields, and results in $I_{\omega_a}<7\times10^8$ W/cm^2 and $I_{\omega_c}<1\times10^3$ W/cm^2. While these conditions were not satisfied by the present experimental parameters, this discrepancy is not serious, as we shall discuss here. Larger electromagnetic fields imply that more population is transferred to states $|2\rangle$ and $|3\rangle$. The term proportional to $\rho_{22}-\rho_{33}$ in the expression for σ_{31} given in Eq. (4b) may not be negligible compared to the first term containing the small quantity $\Delta\tilde{\omega}_{21}$. The numerator of the linear susceptibility becomes $\Delta\tilde{\omega}_{21}(\rho_{11}-\rho_{33})-|\Omega_{32}|^2(\rho_{22}-\rho_{33})/\Delta\tilde{\omega}_{32}^*$, and the denominator takes a more complicated form. In this situation, $\chi^{(1)}(-\omega_c;\omega_c)$ cannot be made zero, although it still has a minimum at $\omega_c=\omega_{21}$. This indicates that an improvement of the ultimate efficiency will be observed, but η at $\omega_c=\omega_{21}$ will be limited by the amplitude of the fields E_{ω_a}, E_{ω_c}, and E_{dc}.

D. Numerical calculation of $\chi^{(1)}$ and $\chi^{(2)}$ for atomic hydrogen

Here we show the numerical results of $\chi^{(1)}$ and $\chi^{(2)}$ for the $n=2-1$ transition in atomic hydrogen. In these cal-

culations we use the field-free basis set $|n,l,m_l\rangle$. State $|1\rangle$ is the $|1s\rangle=|1,0,0,\rangle$ state, $|2\rangle$ is the $|2s\rangle=|2,0,0\rangle$ state, and $|3\rangle\equiv|2p\rangle=|2,1,0\rangle$. The states $|2,1,\pm1\rangle$ having $|m_l|=1$ are not included in the present formulation since they do not contribute to the polarization for linearly polarized light. The atomic levels $|2s\rangle$ and $|2p\rangle$ of hydrogen have the characteristics required by the above theory, namely $|2s\rangle$ is metastable and $|2p\rangle$ is lifetime broadened (with a spontaneous decay rate of $\Gamma=6.26\times10^8$ s^{-1} [11]). The strong coupling between $|2\rangle$ and $|3\rangle$ is given by $H_i^{32}=\mu_{32}E_{dc}=3a_0eE_{dc}=(0.128\ \text{cm}^{-1})E_{dc}$ where E_{dc} is in kV/cm. The calculated energies of states $|1\rangle$, $|2\rangle$, and $|3\rangle$ are $\omega_1=0$, $\omega_2=82\,258.939$ cm^{-1}, and $\omega_3=82\,259.147$ cm^{-1}, respectively (Fig. 1). For this calculation, the relativistic corrections and the Lamb shift [12,13] are added to the energy of the $n=2$ level which in the Bohr model is equal to $I_H-R_H/4=82\,259.36$ cm^{-1}. Here $I_H=109\,678.76$ cm^{-1} is the ionization limit of the hydrogen atom [11], and $R_H=109\,677.58$ cm^{-1} is the Rydberg constant including the reduced mass correction. It is assumed that $\hbar\Omega_{32}$ becomes significantly larger than the spin-orbit splitting, therefore the spin-orbit interaction is neglected.

The calculated values for the susceptibilities in the region of the two-photon resonance are shown in Fig. 2 for six different values of the electric field. A Doppler width of 1.4 cm^{-1} is included in the calculations. Figures 2(a) and 2(b) show the magnitudes of $|\chi^{(2)}|^2$ and $|\chi^{(1)}|^2$, respectively. The real and imaginary parts of $\chi^{(1)}$ are also plotted in Figs. 2(c) and 2(d). At the center of the Stark-split components, i.e., $\omega_c=\omega_{21}$, the value of $|\chi^{(1)}(-\omega_{21};\omega_c)|^2$ quickly approaches zero for increasing fields. This "induced transparency" has its physical origin in the interference due to spontaneous decay of the two closely spaced Stark states (as discussed more fully below, with Fig. 3). On the other hand, the value of $|\chi^{(2)}(-\omega_{21};\omega_a,\omega_a)|^2$ at the center increases for fields up to 7 kV/cm. At higher fields, the peak value of $|\chi^{(2)}|^2$ reaches a constant value and the tuning curve splits into two components, but $|\chi^{(2)}|^2$ still has a reasonably large value at the center; at 27 kV/cm, $|\chi^{(2)}(-\omega_{21};\omega_a,\omega_a)|^2$ maintains about 10% of the peak value. This is because two resonantly enhanced $\chi^{(2)}$ processes interfere constructively at the center. Here, it should be mentioned that the resonance enhancement in the present SHG process results in an extremely large value of the single-atom nonlinear susceptibility at 27 kV/cm. Its peak value was calculated using Eq. (8) and found to be 1.7×10^{-36} m^4/V$\equiv7\times10^{-26}$ esu; and a large value of 5×10^{-37} m^4/V$\equiv2\times10^{-26}$ esu is still maintained at the center. Therefore the ratio $|\chi^{(2)}(-\omega_{21};\omega_a,\omega_a)|\chi^{(1)}(-\omega_{21};\omega_c)|^2$ can become extremely large, indicating a potentially high conversion efficiency. In other words, the best conditions are achieved at the center of the Stark-split components because the absorption becomes exceedingly small for high fields, and the phase-matching condition is exactly satisfied, as shown in Fig. 2(d).

To understand how large an improvement may be obtained in efficiency with increasing electric field, $|\chi^{(1)}|^2$ is shown in Fig. 3 on a semilogarithmic scale. Two important characteristics of the line profiles can be seen in this figure: the Gaussian profile appears as an inverted parabola, and the wings of the Lorentzian line shape are seen extending on each side of the Gaussian profile. At the center of the Stark components, the Doppler profiles are added together, but the Lorentzian profiles interfere des-

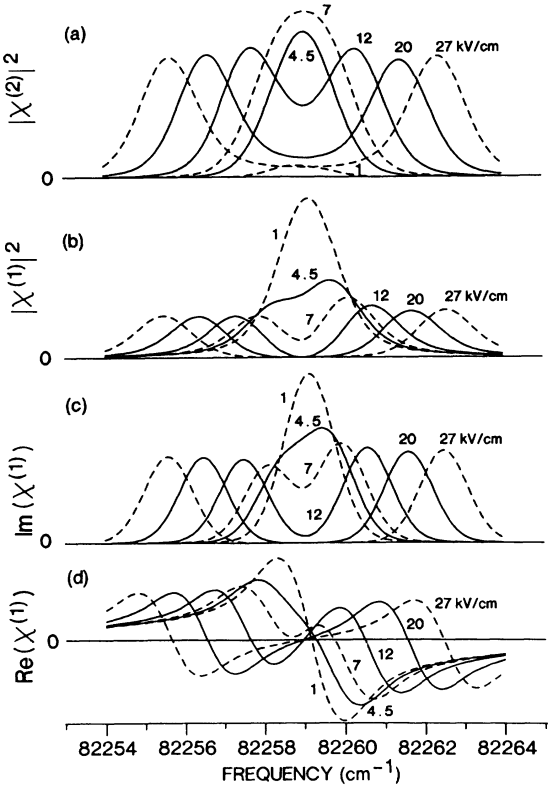

FIG. 2. Frequency dependence of (a) $|\chi^{(2)}|^2$, (b) $|\chi^{(1)}|^2$, (c) imaginary part of $\chi^{(1)}$, (d) real part of $\chi^{(1)}$. The Doppler broadening is included in these calculations.

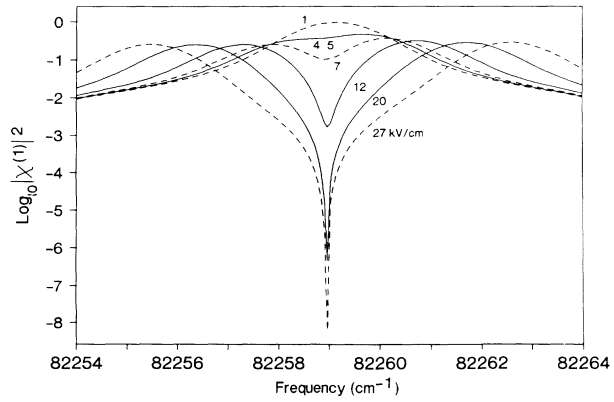

FIG. 3. Frequency dependence of $|\chi^{(1)}|^2$ with logarithmic scale. Doppler broadening of 1.4 cm^{-1} (FWHM) is included in these calculations.

tructively. As the Stark splitting increases, the contributions from the Gaussian distribution of both components rapidly decrease to a small amount, and the destructive interference of the Lorentzian profiles clearly appears. By varying the electric field from 7 to 27 kV/cm, the value of $|\chi^{(1)}(-\omega_{21};\omega_c)|^2$ decreases by seven orders of magnitude. Increasing the electric field also decreases $|\chi^{(2)}(-\omega_{21};\omega_a,\omega_a)|^2$ by a factor of 16. However, if a sufficient interaction length is used in order to allow the SH beam intensity to reach a stationary value, the efficiency η could increase by more than a factor of 10^5.

III. EXPERIMENTAL METHOD

The present experiment was conceived as a simple test of the above theory. For this purpose, it was necessary to measure the incident laser power and frequency in the region of 243 nm, the power of the generated SH radiation near 121.6 nm, and the electric field applied to the H atoms. The one-photon absorption at Lyman-α radiation was measured indirectly by monitoring the number of ions produced by photoionization.

A schematic diagram of the experiment is shown in Fig. 4. Tunable radiation was generated near 486 nm using a dye laser system with coumarin 500 dye (Exciton Chemical Corp.) pumped by a XeCl excimer laser (Lumonics TE-861M-2). The oscillator (of Littman configuration [14]) and two amplifiers were pumped transversely at 7 Hz. Peak powers of up to 350 kW were emitted in pulses of 6-ns duration, and in a linewidth of 0.23 cm^{-1} full width at half maximum (FHWM). This radiation was frequency doubled in a β-barium borate crystal 7 mm in length, generating pulses of 6-ns duration at 243 nm, with peak powers of 45 kW. A quartz prism separated the 486- and 243-nm beams. The frequency of the visible beam was calibrated [15] with an optogalvanic uranium lamp to an accuracy of 0.07 cm^{-1}. A quartz flat reflected 4% of the uv beam into a biplanar phototube (Hamamatsu R1193-02) for power measurements.

The experimental chamber consisted of a six-port cross of stainless steel, evacuated with a diffusion pump (TM-

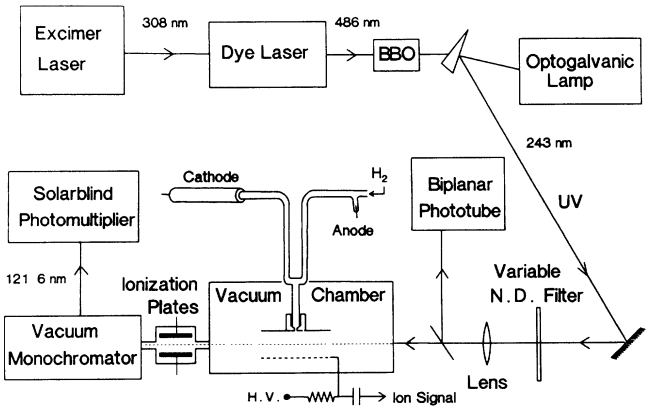

FIG. 4. Experimental arrangement used to study second-harmonic generation in atomic hydrogen with dc electric-field-induced transparency. BBO refers to the nonlinear optical crystal of β-barium borate, and N.D. to the neutral-density filter.

Vacuum Products, Model 641) to a pressure of 2×10^{-6} Torr. The incident linearly polarized laser beam entered the chamber through a quartz window which was 5 mm thick to avoid polarization changes induced by birefringence caused by stress. Hydrogen atoms were generated in a dc glow discharge of H_2 gas placed at the top of the chamber. The discharge was operated at a pressure of 457 mTorr and a current of 50 mA, using commercial ultrahigh-purity-grade gas (Can. Liquid Air Ltd., 99.999%) without further purification. As shown in Fig. 4, a beam of H atoms was directed to the experimental chamber by a pyrex finger (7 cm long) attached near the midpoint between the discharge tube electrodes. The H-atom density was estimated to be $\simeq10^{14}$ cm^{-3}. The Pyrex finger was terminated by an aluminum [16] block 1.5 mm thick, having an aperture 0.9 mm in diameter that served as a nozzle for the H-atom beam. This block and a nickel mesh placed 1.3 mm below served as electrodes for applying a variable dc electric field (up to 27 kV/cm) to the atomic beam. The electric field was calibrated from the measured Stark splitting of the $n=2$ state. The mesh electrode was also used to collect ions produced by three-photon ionization and the resulting signal was ac filtered, amplified, and sent to a boxcar averager (Stanford Research Systems SR250). This signal provided an absolute measurement of the number of photoions produced by the incident beam.

The 243-nm laser beam was focused into the chamber, midway between the electrodes using a lens of 30-cm focal length. At the focal point, the laser beam size was measured to be 38 μm$\times$32 μm FWHM, with Gaussian profiles. The interaction length with the hydrogen beam was measured by translating the hydrogen source in a direction perpendicular to the incident laser beam while monitoring the ion signal, and an interaction length of 2 mm was obtained. Second-harmonic radiation passed through a series of three apertures (3 mm in diameter and spaced by 8 cm), in order to reduce stray scattered light, and was dispersed by a vacuum spectrometer (McPherson 225). For absolute measurements [17] of the vuv radiation power, the baffles were replaced by an ionization cell [18] (Fig. 4) with the transmitted power monitored as the cell pressure of NO was increased.

The entrance and exit slits of the spectrometer were 50 μm wide (giving a spectral resolution of 0.05 nm). A solar-blind photomultiplier (EMR Photoelectric 541G-08-17) was used to measure the power of L_α radiation. The signals were processed with a boxcar averager and stored in a computer. For every experiment, a background measurement was taken by turning off the hydrogen discharge (thus flowing H_2 in the experimental chamber) with all the other parameters unchanged, and this was subtracted from the measured signal.

IV. RESULTS AND DISCUSSION

Experimental data were obtained to confirm the correct behavior of $\chi^{(1)}$ and $\chi^{(2)}$ for the electric-field-induced SHG treated here. First, an investigation of the dependence of SH power on incident laser power was carried out, with good signal-to-noise measurements ob-

tained at $E_{dc}=1200$ V/cm. As expected, the SH power varied as the square of the incident laser power, and was observed to maintain this dependence up to incident powers of ~30 kW. At higher powers, three-photon ionization reduced the density of atoms in the ground state resulting in reduced power of generated SH radiation, and thus all further measurements were carried out at incident powers less than 30 kW. It may be noted that no difference in SH power was discernible when the plane of polarization of the incident beam was either parallel or perpendicular to the applied dc field, but a reduction in SH power by a factor greater than 20 resulted with incident circularly polarized light.

A second set of data measured SH power as a function of the applied field E_{dc}, and was obtained by varying the voltage applied to the mesh electrode. The voltage was ramped through the full range (0–4 kV), with measurements repeated 30 times and averaged, for a laser frequency fixed at $\omega_a=41\,129.47$ cm^{-1} ($2\omega_a$ being in resonance with the unperturbed $2s$ level). The observed dependence of SH power with applied fields up to 27 kV/cm is shown in Fig. 5. For fields up to ~6 kV/cm, the expected quadratic behavior of the power dependence was obtained, but at fields in excess of 7 kV/cm, a decrease of the SH power occurs. It should be mentioned that the decrease becomes slower above 14 kV/cm, and that the SH power at 27 kV/cm is maintained at about 9% of the maximum value at 7 kV/cm.

The above results are well explained by the theoretical behavior of $|\chi^{(2)}|^2$ at the center of two Stark-split components, shown by the solid curve in Fig. 5. It is important to note that the slow decrease above 14 kV/cm is a result of the constructive interference in the $\chi^{(2)}$ process, which maintains the resonantly enhanced $|\chi^{(2)}|$ value at the center, even at high fields. The agreement between the observed and calculated results is even more striking in the observed tuning curves of SH radiation. An example is given in Fig. 6(a) where the measured SH power is plotted as a function of frequency for three different values of the field, $E_{dc}=4.5$, 12, and 20 kV/cm. These curves are seen to be in good agreement with the theoretical results of Fig. 2(a), and in fact reproduce the predicted envelopes in detail. Spectra obtained at other values of E_{dc} also agreed with theoretical predictions. Only one adjustable parameter was used in these calculations, namely the Doppler width, and a value of 1.4 cm^{-1} was necessary to fit the line profiles. This Doppler width corresponds to a temperature of ~300 °C, and is consistent with a measurement of the fluorescence linewidth.

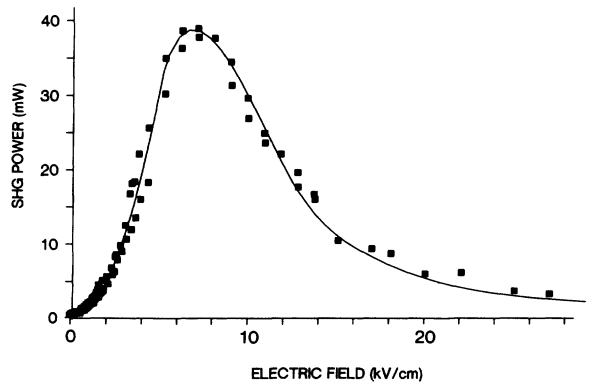

FIG. 5. Second-harmonic power at the resonance frequency as a function of the applied electric field E_{dc} for fields up to 27 kV/cm, with incident power of 35 kW. The solid curve shows the predicted dependence.

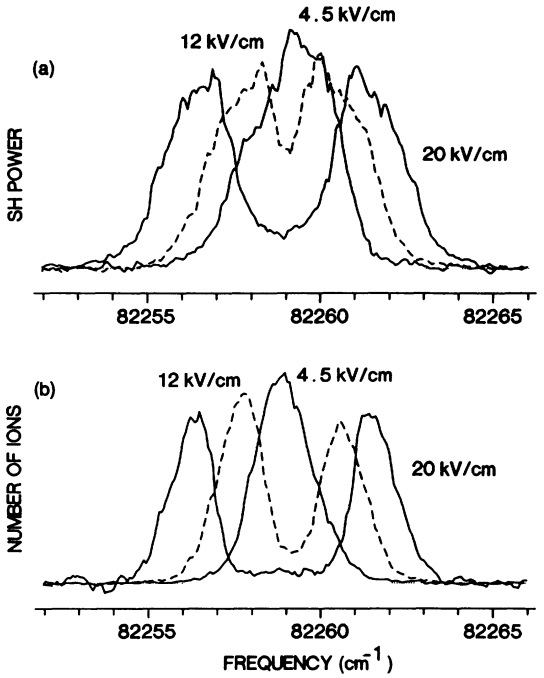

FIG. 6. Frequency dependence of (a) second-harmonic power, (b) ion signal. These results were obtained for $E_{dc}=4.5$, 12, and 20 kV/cm, and incident power of 30 kW.

Thus we have demonstrated the $|\chi^{(2)}|^2$ behavior experimentally via the tuning curve of SH power. Also, it would be important to estimate experimentally the absolute $|\chi^{(2)}|$ value from the measurement of the SHG conversion efficiency under the present conditions of low density and short interaction length. The conversion efficiency was $I_{SH}/I_0=9.3\times10^{-7}$ obtained with 30-kV incident power, generating 28 mW of SH radiation at $\omega_c=82\,259.0$ cm^{-1}. The measurement was carried out at a field $E_{dc}=7$ kV/cm, corresponding to the field at which $|\chi^{(2)}|^2$ is the largest, Fig. 2(a). With this value of the conversion efficiency, and experimental parameters $L=2.1$ mm, $I_0=3\times10^9$ W/cm^2 (30 kW focused to a 35-μm spot), and $N_H=10^{14}$ atoms/cm^3, the single-atom $|\chi^{(2)}|$ was calculated to be 2×10^{-36} m^4/V$\equiv8\times10^{-26}$ esu at this field, in excellent agreement with the theoretical value of 1.7×10^{-36} m^4/V (cf. Sec. II D).

Finally, in order to confirm the predicted behavior of $\chi^{(1)}$, an alternative to absorption measurements was necessary since the slight absorption detected at the peaks of the SHG tuning curves was inadequate for obtaining accurate values. Thus estimates of absorption were provided by simultaneous measurements of SH power and photoions produced by the incident beam.

First, we discuss how the number of ions is related to an absorption measurement. The ions are produced in a two-step process: two-photon absorption ($2\omega_a$) from the ground state followed by one-photon (ω_a) ionization. To calculate the number of ions, we assume that the one-photon ionization rate from states $|2\rangle$ and $|3\rangle$ is independent of frequency within the 10-cm^{-1} tuning range of interest in the present work. Therefore the observed three-photon ionization is proportional to two-photon absorption from the ground state, which is determined from the imaginary part of the two-photon term of the polarization given in Eq. (5), namely

$$\mathrm{Im}(\sigma_{21}\mu_{12})=\mathrm{Im}\left[\frac{\Delta\tilde{\omega}_{31}}{2\Delta\tilde{\omega}_{21}\Delta\tilde{\omega}_{31}-2|\Omega_{32}|^2}\mu_{12}\Omega_{21}\right]. \quad (12)$$

Equation (12) has some similarity to Eq. (7), but here $\Delta\tilde{\omega}_{31}$ instead of $\Delta\tilde{\omega}_{21}$ appears in the numerator. This implies that the two-photon absorption (and thus the ion signal) will closely follow the imaginary part of $\chi^{(1)}$, but without an exact zero at the center of the two components. A small contribution occurs because state $|3\rangle$ has a nonzero radiative decay rate, and therefore $\Delta\tilde{\omega}_{31}\neq 0$. With Doppler broadening included in this strongly coupled system, the difference between the absorption of two photons at ω_a and of one photon at ω_c becomes relatively small. Thus we conclude that measurement of the photoion signal is equivalent to one-photon absorption, and is far more sensitive experimentally.

We now compare the experimental results of photoions produced, given in Fig. 6(b) with the calculated imaginary part of $\chi^{(1)}$ or photon absorption, given by Eq. (7) and shown in Fig. 2(c). The important features of the experimental curves, such as frequencies and amplitudes of the peaks, are well reproduced by the theoretical curves. Here, we point to the significant decrease of ion signal or absorption at the center of the Stark components to essentially zero with increasing field. A detailed examination of ion measurements revealed that while the signal at the center of the Stark components drops to ~3% of the peak value, it remains at this value for applied fields greater than 20 kV/cm, instead of reducing to zero. A possible experimental reason for this residual signal is that it is caused by ionization of hydrogen atoms located outside the region delimited by the electrodes, but in the path of the incident laser beam. In this region of lower (fringe) electric fields, the Stark levels are split by a smaller amount, but ionization may occur producing a constant background of ions. Therefore, in comparing the measured signals with the calculated values based on $\mathrm{Im}|\chi^{(1)}(-\omega_{21},\omega_c)|$, the background of 3% was subtracted from the measured signal at 27 kV/cm. The corrected values are plotted in Fig. 7, which presents the dependence of ion signal on applied electric field. It is seen that the calculated dependence of $\chi^{(1)}(-\omega_{21};\omega_c)$ closely follows the measured ion signal as it quickly decreases with increasing field, and at 20 kV/cm becomes less than 1% of the maximum observed with small fields. This is in strong contrast to the behavior of $\chi^{(2)}$, which remains at ~40% of its maximum value, on resonance. It should be noted that the observed reduction of ion signal is not due simply to the separation of the Stark components, nor to competition between harmonic generation and multiphoton ionization processes [19,20], since the atomic density and absorption in the present experiments were insufficient for such competitive processes.

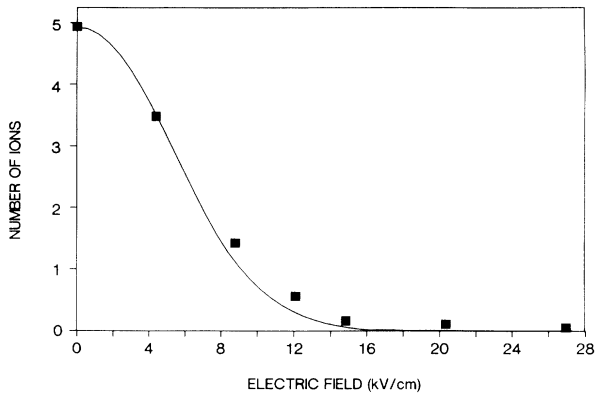

FIG. 7. Measured number of ions corrected for the 3% background as a function of the electric field. The solid curve shows $|\chi^{(1)}(-\omega_{21};\omega_c)|$.

In the present experiments, the interaction length and density were insufficient to allow the generated SH wave to reach a stationary value, so that the ultimate efficiency η defined in Eq. (11) could not be determined. However, from the above good agreement between experiment and theory for $\chi^{(2)}$ and $\chi^{(1)}$, the conditions for achieving high conversion efficiency should be realized in the present SHG process with atomic hydrogen.

V. CONCLUSION

In summary, it has been shown theoretically that coupling of a metastable state and a nearby upper state with a strong applied electric field can resonantly enhance the nonlinear susceptibility of a medium and simultaneously induce transparency and a zero contribution of the resonance transition to the refractive index. The behavior is equivalent to the coupling by a strong electromagnetic field which was first predicted by Harris, Field, and Imamoğlu [8]. These theoretical results were applied to the coupling of the $2s$ and $2p$ states of atomic hydrogen, and the values of $\chi^{(1)}$ and $\chi^{(2)}$ as a function of frequency were determined showing their dependence on the applied field.

The theoretical predictions for $\chi^{(1)}$ and $\chi^{(2)}$ were tested and confirmed experimentally by measurements of second-harmonic generation at Lyman α in atomic hydrogen. In particular, evidence for enhanced SHG and reduced absorption was obtained. A conversion efficiency of $\sim 10^{-6}$ was observed in a 2-mm interaction length at a density of 10^{14} atoms/cm^3. From a simulation of the scaling characteristics of the SHG process and us-

ing Eq. (11) together with the present data, it is expected that the efficiency can be improved by several orders of magnitude [21], and lead to a powerful source of coherent radiation at Lyman α. While the present work has dealt with a simple atomic system in the gaseous state, this theory should be applicable to molecular media as well as to the liquid and solid states.

ACKNOWLEDGMENTS

This research was supported by the Natural Sciences and Engineering Research Council, the Premier's Council Technology Fund, and the University of Toronto. L. M. is grateful to the University of Toronto for financial support during the course of this study.

*Permanent address: Department of Applied Physics and Chemistry and Institute for Laser Science, University of Electro-Communications, Chofu, Tokyo 182, Japan.

[1] V. G. Arkhipkin and Yu. I. Heller, Phys. Lett. **98A**, 12 (1983).

[2] S. E. Harris, Phys. Rev. Lett. **62**, 1033 (1989); in *Short Wavelength Coherent Radiation: Generation and Applications,* edited by R. W. Falcone and J. Kirz (Optical Society of America, Washington DC, 1988), Vol. 2. p. 414.

[3] M. D. Scully, Shi-Yao Zhu, and A. Gavrielides, Phys. Rev. Lett. **62**, 2813 (1989).

[4] A. Imamoğlu, Phys. Rev. A **40**, 2835 (1989).

[5] S. E. Harris and J. J. Macklin, Phys. Rev. A **40**, 4135 (1989).

[6] A. Imamoğlu and S. E. Harris, Opt. Lett. **14**, 1344 (1989).

[7] G. S. Agarwal, S. Ravi, and J. Cooper, Phys. Rev. A **41**, 4721 (1990); **41**, 4727 (1990).

[8] S. E. Harris, J. E. Field, and A. Imamoğlu, Phys. Rev. Lett. **64**, 1107 (1990).

[9] A. Imamoğlu, J. E. Field, and S. E. Harris, Phys. Rev. Lett. **66**, 1154 (1991).

[10] K. Hakuta, L. Marmet, and B. P. Stoicheff, Phys. Rev. Lett. **66**, 596 (1991).

[11] I. I. Sobelman, *Atomic Spectra and Radiative Transitions* (Springer-Verlag, New York, 1979).

[12] C. Cohen-Tannoudji, B. Diu, and F. Laloë, *Quantum Mechanics* (Wiley, New York, 1977).

[13] E. U. Condon and G. H. Shortley, *The Theory of Atomic Spectra* (Cambridge University Press, Cambridge, 1987).

[14] M. G. Littman, Opt. Lett. **3**, 138 (1978).

[15] B. A. Palmer, R. A. Keller, and R. Engleman, Los Alamos Science Laboratory–University of California, Report No. LA-8251-MS, UC34A, 1980 (unpublished).

[16] B. J. Wood and H. Wise, J. Chem. Phys. **29**, 1416 (1958).

[17] J. A. R. Samson, *Techniques of Vacuum Ultraviolet Spectroscopy* (Wiley, New York, 1967).

[18] P. R. Herman and B. P. Stoicheff, Opt. Lett. **10**, 502 (1985).

[19] J. J. Wynne, Phys. Rev. Lett. **52**, 751 (1984).

[20] P. R. Blazewicz, M. G. Payne, W. R. Garret, and J. C. Miller, Phys. Rev. A **34**, 5171 (1986); P. R. Blazewicz and J. C. Miller, *ibid.* **38**, 2863 (1988), and references therein.

[21] We have recently realized an enhancement of 100 by using a larger density-length product.